

Quasiperiodic ELF/VLF Emissions Detected Onboard the DEMETER Spacecraft: Theoretical Analysis and Comparison With Observations

D L Pasmanik, A G Demekhov, M Hayoš, F Němec, O Santolík, Michel Parrot

▶ **To cite this version:**

D L Pasmanik, A G Demekhov, M Hayoš, F Němec, O Santolík, et al.. Quasiperiodic ELF/VLF Emissions Detected Onboard the DEMETER Spacecraft: Theoretical Analysis and Comparison With Observations. Journal of Geophysical Research Space Physics, 2019, 124, pp.5278-5288. 10.1029/2018JA026444 . insu-03217036

HAL Id: insu-03217036
https://insu.hal.science/insu-03217036

Submitted on 4 May 2021

HAL is a multi-disciplinary open access archive for the deposit and dissemination of scientific research documents, whether they are published or not. The documents may come from teaching and research institutions in France or abroad, or from public or private research centers.

L'archive ouverte pluridisciplinaire **HAL**, est destinée au dépôt et à la diffusion de documents scientifiques de niveau recherche, publiés ou non, émanant des établissements d'enseignement et de recherche français ou étrangers, des laboratoires publics ou privés.

Check for updates

AGU100 ADVANCING EARTH AND SPACE SCIENCE

JGR Space Physics

RESEARCH ARTICLE
10.1029/2018JA026444

Quasiperiodic ELF/VLF Emissions Detected Onboard the DEMETER Spacecraft: Theoretical Analysis and Comparison With Observations

D. L. Pasmanik[1], A. G. Demekhov[1,2], M. Hayoš[3], F. Němec[4], O. Santolík[3,4], and M. Parrot[5]

[1]Institute of Applied Physics, Russian Academy of Sciences, Nizhny Novgorod, Russia, [2]Polar Geophysical Institute, Apatity, Russia, [3]Department of Space Physics, Institute of Atmospheric Physics, The Czech Academy of Sciences, Prague, Czech Republic, [4]Faculty of Mathematics and Physics, Charles University, Prague, Czech Republic, [5]LPC2E/CNRS, Orléans, France

Key Points:
- Numerical simulation of QP emissions for a wide range of plasma parameters is performed
- Theoretical results are in a good agreement with DEMETER spacecraft observations
- A realistic choice of radial profile of cold plasma density is important for this agreement

Correspondence to:
D. L. Pasmanik,
pdl@aurora.appl.sci-nnov.ru

Citation:
Pasmanik, D. L., Demekhov, A. G., Hayosh, M., Němec, F., Santolík, O., & Parrot, M. (2019). Quasiperiodic ELF/VLF emissions detected onboard the DEMETER spacecraft: Theoretical analysis and comparison with observations. *Journal of Geophysical Research: Space Physics*, *124*, 5278–5288. https://doi.org/10.1029/2018JA026444

Received 24 DEC 2018
Accepted 11 JUN 2019
Accepted article online 25 JUN 2019
Published online 13 JUL 2019

Abstract We present results of numerical simulation of quasiperiodic (QP) extra low frequency/very low frequency emissions performed by using a theoretical model of flow cyclotron maser based on a self-consistent set of equations of the quasi-linear plasma theory averaged over oscillations of waves and particles in a geomagnetic flux tube. Calculations were made for a wide range of plasma parameters (i.e., cold plasma density, *L*-shell, and energetic electron flux) in order to obtain a statistical relationship between various properties of QP emissions, such as the repetition period, the frequency bandwidth, the frequency drift rate, and the characteristic wave spectral energy density. The theoretical results are compared with the results of a statistical study of QP emissions measured by the DEMETER spacecraft (Hayosh et al., 2014, https://doi.org/10.1002/2013JA019731). The simulation results are in a good agreement with the observation data in the case of reasonable choice of cold plasma density value and its dependence on the QP-source location (*L*-shell). In particular, an increase in the frequency bandwidth of QP very low frequency waves with increasing central frequency of QP emissions, a decrease in the frequency drift rate of QP elements with increasing repetition period, and a decrease in the characteristic wave spectral energy density with increasing repetition period are confirmed.

1. Introduction

Wide band emissions characterized by a periodic modulation of the wave intensity with typical periods from several seconds up to a few minutes are called quasiperiodic (QP) whistler emissions. They are observed inside the plasmasphere or near the plasmapause (see, e.g., Hayakawa & Sazhin, 1992; Helliwell, 1965; Němec et al., 2018; Sato et al., 1974; Sazhin & Hayakawa, 1994; Smith et al., 1998). Generation of QP emissions is sometimes observed to be accompanied by precipitation of energetic electrons, which is also modulated with the same period (Hayosh et al., 2014).

Modulation of the wave intensity of QP emissions is sometimes associated with geomagnetic pulsations of the same period, corresponding to Pc3–Pc5 pulsations (Manninen et al., 1994; Morrison, 1990; Němec et al., 2013). Such QP emissions are called QP1. QP events which do not correlate with geomagnetic pulsations are called QP2 class (Sato et al., 1974). Both types of QP emissions are related to development of the cyclotron instability. In the case of QP1 events, which are typically observed during magnetically disturbed conditions, a quasiperiodic modulation of the cyclotron instability conditions is provided by geomagnetic pulsations (Chen, 1974; Kimura, 1974; Sato & Fukunishi, 1981; Sazhin, 1987).

The mechanism of QP2 emission generation was proposed by Bespalov and Trakhtengerts (1976) and Davidson (1979) on the basis of a self-consistent quasi-linear plasma theory for cyclotron interactions. It was shown that in the presence of a constant source of energetic electrons with transverse anisotropic distribution function, a relaxation oscillations regime of wave generation can exist. With a further development of this model by Bespalov (1981), a regime of self-sustaining oscillations was obtained.

A more rigorous kinetic model of the flow cyclotron maser (FCM) was developed by Trakhtengerts et al. (1986). Demekhov and Trakhtengerts (1994) demonstrated the ability of this model to explain main

©2019. American Geophysical Union. All Rights Reserved.

properties of QP emissions including typical repetition periods and the frequency drift within individual elements. Pasmanik et al. (2004a) studied the dependence of the emission properties on the model parameters, and Pasmanik et al. (2004b) successfully used this model to reproduce several specific QP events observed by Freja and Magion 5 satellites. In the latter paper, an algorithm for estimation of plasma parameters that are not directly available from satellite measurements, on the basis of QP emission properties, was suggested.

QP emissions are known to spread considerably across L-shells (see, e.g., Manninen et al., 2018; Němec et al., 2018; Titova et al., 2015), which indicates their propagation in nonducted mode. However, their generation is related to the guided propagation in the source flux tube. This is confirmed, for example, by calculations of the wave growth rate in the source region (Lyubchich et al., 2017), which yield a one-hop gain ~1, thereby indicating the importance of several hops for the considerable wave growth. Bespalov et al. (2010) and Manninen et al. (2014) also argued in favor of guided propagation by revealing fine periodic structure of QP elements with the periods corresponding to the two-hop propagation time of whistler mode waves. Němec et al. (2018) showed that QP emission frequencies are almost always below one half of the equatorial electron gyrofrequency, which also indirectly confirms the importance of guided propagation for their generation.

Results for direct simultaneous observations of QP emissions and accompanying energetic electron precipitation and analysis of their correlation for three events observed by the low-orbiting DEMETER spacecraft were presented by Hayosh et al. (2014). Based on the observed correlation between bursts of wave intensity and energetic particle flux, the location and spatial extent of the source region for QP emissions were estimated.

Hayosh et al. (2014) performed a detailed statistical study of QP emissions observed by the DEMETER spacecraft. Very low frequency data measured during all 6 years of the satellite operation were used to select QP emissions events in the frequency range from 15 Hz to 17.4 kHz with modulation periods higher than 10 s and with frequency bandwidths higher than 200 Hz. Each event was manually processed to identify QP elements, and their properties, such as the frequency bandwidth, the frequency drift rate, and the characteristic wave spectral energy density, were obtained. The analysis of this data set allowed them to obtain statistical relationships between the mentioned parameters of QP emissions.

In this paper, we present the results of theoretical modeling of QP emissions for a wide range of plasma parameters, and we compare the obtained results with the experimental results of Hayosh et al. (2014).

2. Theoretical Model

We use a FCM model for numerical simulations of QP emissions in the paper. This model is based on a self-consistent set of equations of the quasi-linear plasma theory for the distribution function of energetic electrons $F(\mu, v, t)$ and whistler wave spectral energy density $\varepsilon(\omega, t)$:

$$\frac{\partial F}{\partial t} = \frac{1}{T_b}\frac{\partial}{\partial \mu}\mu D\frac{\partial F}{\partial \mu} + J, \tag{1}$$

$$\frac{\partial \varepsilon}{\partial t} = \frac{2}{T_{\mathrm{gr}}}\left(\Gamma - |\ln R|\right)\varepsilon, \tag{2}$$

where $\mu = \sin^2\Theta_L$, Θ_L is the equatorial pitch angle, v is the electron velocity, T_b is the bounce-oscillation period, D is the coefficient of pitch-angle diffusion, J describes the effective source of energetic electrons, Γ is the one-hop gain of whistler waves on the pass between conjugate ionospheres, T_{gr} is the period of wave-packet bounce oscillations between conjugate ionospheres, and R is the effective reflection coefficient describing wave energy losses. Details of the reflection process of the QP emissions have been described by Hanzelka et al. (2017).

Note that equations (1) and (2) are obtained by averaging the basic quasi-linear equations over particle bounce oscillations between the mirror points and wave-packet oscillations between conjugate ionospheres, as well as over the cross section of the interaction region. Therefore, they assume guided wave propagation in the generation region and slow temporal variations compared to characteristic particle and wave bounce time scales which are about one to several seconds for the very low frequency waves in the inner magnetosphere. Details of the derivation can be found in Demekhov and Trakhtengerts (1994), Pasmanik et al. (2004a), and Trakhtengerts and Rycroft (2008).

The diffusion coefficient D is determined by the wave spectral energy density ε, and in turn, the wave gain Γ is determined by the electron distribution function F, assuming wave-particle interactions via the first-order cyclotron resonance:

$$D(\mu, v, t) = \int G_1(\omega, \mu, v)\varepsilon(\omega, t)\mathrm{d}\omega, \tag{3}$$

$$\Gamma(\omega, t) = \int G_2(\omega, \mu, v)\left(\mu\frac{\partial F}{\partial \mu} - \frac{\omega}{\omega_{HL}}F\right)d^3v, \tag{4}$$

where G_1 and G_2 are known functions (see Pasmanik et al., 2004a), ω_H is the electron gyrofrequency, and the subscript "L" refers to values in the equatorial plane. Equations (3) and (4) make systems (1) and (2) self-consistent, that is, a variation in the wave spectral energy density $\varepsilon(\omega, t)$ results in the change of the distribution function of energetic electrons $F(\mu, v, t)$ and vice versa. In particular, an increase in the frequency of $\varepsilon(\omega, t)$ maximum is related to a shift of the $\partial F/\partial\mu$ maximum to higher pitch angles due to pitch-angle diffusion (see Demekhov & Trakhtengerts, 1994, for more detail).

As the source of free energy, the injection of energetic electrons with anisotropic velocity distribution into the interaction region is considered. Such injection occurs due to the magnetic drift of electrons across the geomagnetic field in the equatorial plane. The same process is responsible for removal of energetic particles from the interaction region. Both mechanisms are taken into account in the term $J(\mu)$, which is determined by the difference of the pitch-angle distributions of energetic particles drifting into and away from the interaction region. Note that another mechanism of energetic particles loss, which is related to precipitation via the loss cone, also exists, but it is neglected in this paper.

Following Pasmanik et al. (2004a), we use the approximation of a monoenergetic electron distribution:

$$\Phi(\mu, v, t) = (2\pi v_0^2)^{-1}\delta(v - v_0)\tilde{\Phi}(\mu, t), \tag{5}$$

where $v_0 = \sqrt{2W_0/m}$, and W_0 is the characteristic energy of energetic electrons, and consider only waves propagating along the geomagnetic field ($\vec{k}\|\vec{B}$). As was discussed by Bespalov and Trakhtengerts (1976), Demekhov and Trakhtengerts (1994), and Pasmanik et al. (2004a, 2004b), the inhomogeneous geomagnetic field provides a spread in resonant energies of particles interacting with a wave of a given frequency ω, and moreover, the growth rate of ducted whistler waves is determined by integral parameters of the energy distribution (such as characteristic energy and particle flux). Thus, the use of this approximation does not lead to significant changes in the wave spectrum dynamics and allows us to obtain correct values and dynamic properties of the spectrum, energetic particle flux, and pitch-angle distribution.

The source pitch-angle distribution was chosen in the form

$$F_{\mathrm{in}} = \begin{cases} C\sin(\frac{\pi}{2}æ/\rho_0)\,, & æ \le æ_0 \\ C\,, & æ > æ_0 \end{cases}, \tag{6}$$

where $æ \equiv \sqrt{\mu}$; the parameter $æ_0$ characterizes the steepness of energetic particles distribution. The constant C is determined by the energetic plasma density N_h, which is obtained by integrating (5) over the velocity space: $N_h = \int F_{\mathrm{in}}\sin\Theta_L\mathrm{d}\Theta_L$.

The main parameters of the model are L-shell (which determines, in particular, the values of T_b and ω_{HL} in equations (1) and (2)), cold plasma density N_{cL} (which together with L determines the value of T_{gr}), energetic plasma density N_h, characteristic energy W_0, anisotropy of pitch-angle distribution of energetic electrons, and effective wave reflection coefficient R that quantifies wave energy losses.

Equations (1)–(4) can easily be modified to take into account the effect of geomagnetic flux tube oscillations on the whistler cyclotron instability (Bösinger et al., 1996). However, we do not have any information on the presence or absence of such geomagnetic pulsations during the QP events analyzed by Hayosh et al. (2014). Therefore, we performed the simulations only without the effect of geomagnetic pulsations, that is, by assuming these events to be of QP2 type. Two facts speak in favor of this assumption. First, the QP events of Hayosh et al. (2014) were predominantly observed during quiet geomagnetic conditions. Second, the spectra of the most of the observed QP emissions were typical for QP2 events, that is, they had a clear frequency drift which varied in time.

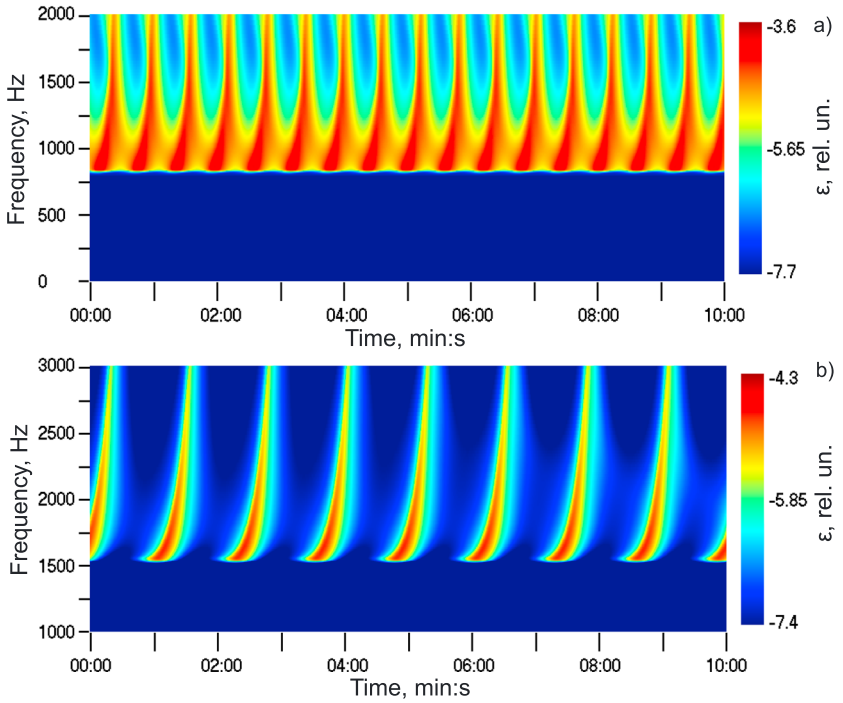


Figure 1. The results of numerical simulation of the quasiperiodic events by using the flow cyclotron maser model. (a) and (b) correspond to the cases presented in Figures 1a and 1b of Hayosh et al. (2014), respectively. See the text for the model parameter values.

3. Results of Numerical Simulations

3.1. Simulation of Specific Events

Following Hayosh et al. (2014), we first present results of a numerical simulation of specific examples of QP emissions observed by DEMETER spacecraft (see Figure 1 in that paper).

The model parameters were chosen by using the algorithm described by Pasmanik et al. (2004b). We only briefly repeat it here referring to this paper for details. At first, L-shell was estimated based on the assumption that the QP emissions were observed near the L-shell of their generation region. Since the spacecraft passed a wide range of L-shells during the event, the value corresponding to the maximum wave amplitude was chosen. The actual location of the source region could be at different L-shell than we get from this assumption. However, it is the only possible way of estimating the source location based on the available data from DEMETER data for a statistical study. Then a guess value for the cold plasma density N_{cL} was taken from a plasmaspheric electron density model (Ozhogin et al., 2012). After that, the energy W_0 of energetic particles could be estimated from the expression for the lowest frequency of the generation band, which is determined by the cyclotron resonance condition in the equatorial plane (Pasmanik et al., 2004b)

$$\omega_0 = \omega_{HL}/\beta_*, \quad \beta_* = \left(\frac{\omega_{pL} v_0}{\omega_{HL} c}\right)^2 = N_{cL} W_0 \left(\frac{8\pi e^2}{m^2 c^2 \omega_{HL}^2}\right). \tag{7}$$

Here ω_{pL} is equatorial electron plasma frequency, e and m are the electron charge and mass, and c is the speed of light. The remaining model parameters could not be estimated on the basis of the available measurement data. Therefore, we chose them in order to achieve the best match for the spectral and temporal patterns of the observed and simulated QP emissions.

Examples of the spectrograms obtained by using the FCM model are shown in Figure 1. Figure 1a demonstrates the results of modeling of the event with QP emissions observed by DEMETER on 1 September 2004 between 06:59:00 UT and 07:09:10 UT in the Northern Hemisphere at MLat from about 65° to 40° (hereafter called case A, see Figure 1a in Hayosh et al., 2014). The QP emissions were observed at frequencies between about 800 and 1,900 Hz, and the repetition period was about 35 s. The following values of model parameters

were used: $L = 4.0$, $N_{cL} = 220$ cm^{-3}, $W_0 = 46$ keV and $N_h = 0.24$ cm^{-3}, æ$_0 = 0.2$ (these values correspond to the energetic electron flux of about $S \approx 2 \cdot 10^7$ cm^{-2} s^{-1}), and $|\ln R| = 2$.

It is seen that with use of FCM model, we can obtain QP emissions with required properties: the repetition period of QP elements of about 35 s, the frequency drift rates of about 30 Hz/s (at frequencies below 1,250 Hz) and of about 85 Hz/s (at frequencies above 1,250 Hz), the wave spectral energy density modulation is by 1–2 orders of magnitude, and the lower frequency is about 800 Hz. As discussed in Sec. 3 of Demekhov and Trakhtengerts (1994), at the initial stage of QP element generation, the wave spectrum is determined by the frequency profile of the growth rate calculated for a distribution function not affected by the waves, that is, by the energetic particles supplied by the source. In the case $\beta_* \gg 1$ and a moderate or weak pitch-angle anisotropy, this frequency is close to the lower boundary of the generation band given by equation (7) (Demekhov & Trakhtengerts, 1994; Trakhtengerts & Rycroft, 2008). This is the reason why the spectrum of a QP element initially peaks at low frequencies and subsequently evolves to higher frequencies. This evolution, as it was shown by Demekhov and Trakhtengerts (1994) and Pasmanik et al. (2004a), is related to the quasi-linear modification of the electron distribution function during the wave generation which, in turn, modifies the frequency spectrum of the wave growth rate.

The main discrepancy between the modeling and observation results is for the upper frequency which is about 3 and 1.9 kHz, respectively (the frequency range in Figure 1a is limited to 2 kHz for consistency with Figure 1a in Hayosh et al., 2014). This could be related to the peculiarities of the wave propagation from the source to the point of their detection (Hayosh et al., 2016; Němec et al., 2014; Němec, Bezděková, et al., 2016; Němec, Hospodarsky, et al., 2016). In particular, the wave ducting becomes less efficient, and therefore, effective losses could increase as the frequency approaches one half of the electron gyrofrequency at the equator (which is equal to ≈6.9 kHz for $L = 4.0$).

Figure 1b shows the results of modeling for the second case of QP emissions observed on 13 April 2010 between 06:16:15 UT and 06:26:30 UT in the Southern Hemisphere at MLat from about 50° to 62° at frequencies between about 1,500 and 2,800 Hz, with a repetition period of about 75 s. The model parameters in this case were $L = 4.3$, $N_{cL} = 165$ cm^{-3}, $W_0 = 17$ keV and $N_h = 0.16$ cm^{-3} (energetic electron flux of about $S \approx 1 \cdot 10^7$ cm^{-2} s^{-1}), $|\ln R| = 2$, and æ$_0 = 0.2$.

In this case, we obtained the QP emission with the lower frequency of about 1,500 Hz, the repetition period of about 75 s, and the frequency drift rates of about 8 Hz/s (at frequencies below 1,900 Hz) and of about 35 Hz/s (at frequencies above 1,900 Hz). The wave spectral energy density modulation in this case is of about 2 orders of magnitude with a more clear separation of QP elements as compared to the case A. This difference conforms well to the observations. Similar to the simulation of the case A, the upper frequency is higher (about 4.5 kHz) than in the observation.

Let us note that due to the absence of measurements of plasma parameters near the equatorial plane, there is an ambiguity in the model parameters, and it is possible to obtain QP emissions with similar characteristics for different combination of model parameters. For example, we can use different N_{cL} and W_0 values and keep the product $N_{cL}W_0$ constant in order to match the lowest frequency of the generation. In this case, some other model parameters (e.g., æ$_0$) have also to be varied to ensure the best matching of the dynamic spectrum shape. A different L-value can be also used with proper modification of other model parameters.

3.2. Comparison of the Simulation Results With Statistical Parameters of QP Emissions Observed by DEMETER

In order to compare the simulation results from the FCM model with the results of the statistical analysis of observation data, we built a database of numerical modeling results for a large set of model parameters within the following limits: $L = 3.5$–5.5, $N_{cL} = 30$–600 cm^{-3}, $W_0 = 8$–64 keV, $N_h = 0.04$–0.64 cm^{-3}, and æ$_0 = 0.2$–0.7. We used uniform grids for L and æ$_0$ and logarithmically spaced grid for N_{cL}, W_0, and N_h. In total, we performed about 5,500 simulation runs with different sets of parameters.

For each model run with a given parameter combination, the existence of the QP regime of wave generation was checked by using an automated procedure based on the analysis of wave intensity variation. For the runs with the identified QP regime, we calculated the same characteristics as were determined for the observation data by Hayosh et al. (2014): the repetition period T, the upper and lower frequencies of QP elements, the frequency bandwidths Δf, the frequency drift rate df/dt, and the characteristic wave spectral energy density

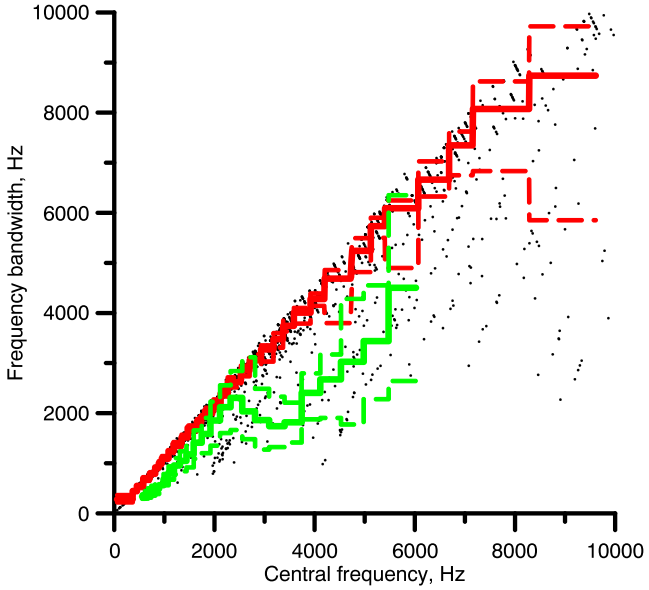


Figure 2. The dependence of the frequency bandwidth on the central frequency obtained from the results of numerical simulations for the entire set of simulation variants. Solid red lines correspond to the median of the frequency bandwidth, and dashed red lines correspond to the lower and upper quartiles. Solid and dashed green lines show, respectively, the median and the lower and upper quartiles for the corresponding statistical results of Hayosh et al. (2014).

ε_0. To calculate the latter, the maximum wave spectral energy density values (over all frequencies) at each time step during a QP element were taken, and then the median value for this set was computed.

The set of model parameter combinations used in our simulations is not necessarily the same as the distribution of plasma parameters in the magnetosphere during the observations presented by Hayosh et al. (2014). Thus, we will not discuss their results related to the number of observed QP events but instead focus on the interrelation between various parameters of QP emissions.

The relationship between the frequency bandwidth and the central frequency (calculated as the half-sum of the minimum and the maximum frequencies) of QP emissions is shown in Figure 2. This dependence is plotted for the entire set of simulation variants. Hereinafter, each point on the plot corresponds to a single simulation run for a given combination of model parameters. Solid red line corresponds to the median of the frequency bandwidth, and dashed red lines correspond to the lower and upper quartiles. It is seen that the spread in the frequency bandwidth increases with an increase in the central frequency. The maximum value of the bandwidth is a bit higher than but close to the central frequency. The minimum value of the bandwidth becomes much lower than the central frequency as the latter increases. In order to visually compare these results with the observation analysis results of Hayosh et al. (2014), we overplotted the median and upper and lower quartiles from their Figure 4b as green lines (solid and dashed, respectively). The obtained relationship is in a good agreement with the results of Hayosh et al. (2014). However, a larger spread in a frequency bandwidth was obtained from the observation data. This could be explained by the fact that DEMETER spacecraft was lower orbiting and observed the emissions far away from the generation region located near the geomagnetic equatorial plane. Thus, the observed frequencies of QP emissions could be strongly affected by the wave propagation from the source to the point of their detection. An example of such an effect was given, for example, by Titova et al. (2015).

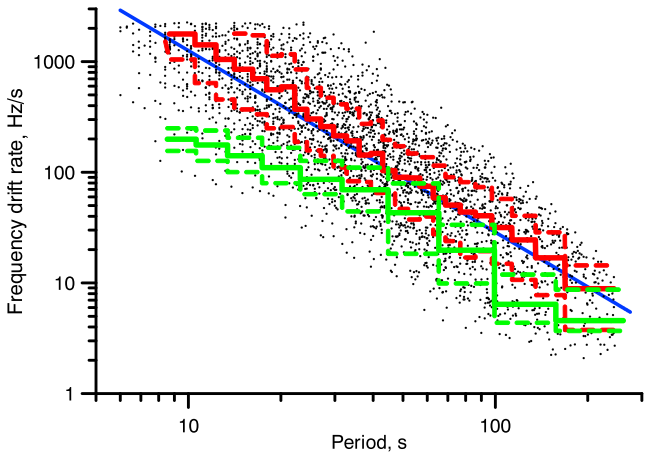


Figure 3. The dependence of the frequency drift rate of the quasiperiodic element on the repetition period of emissions obtained from the results of numerical simulations for the entire set of simulation variants. Solid red lines correspond to the median of the frequency drift rate, and dashed red lines correspond to the lower and upper quartiles. Blue line is a power law approximation with the exponent equal to −1.6. Similar to Figure 2, solid and dashed green lines show, respectively, the median and the lower and upper quartiles for the corresponding statistical results of Hayosh et al. (2014).

The relationship between the frequency drift rate of a QP element and the repetition period of emissions obtained from numerical simulations is shown in Figure 3. Similar to Figure 2, this dependence is plotted for the entire set of the simulation variants. Solid red line corresponds to the median of the frequency drift rate, and dashed red lines correspond to the lower and upper quartiles. Blue line is a power law least-square approximation with the exponent equal to −1.6. Similar to Figure 2, the results of the statistical analysis of corresponding observation data from Hayosh et al. (2014) are plotted as green lines. The obtained dependence is in a fairly good agreement with the results of observation data analysis, where the power law approximation with the exponent equal to −1.2 was obtained (see Figure 6a in Hayosh et al., 2014).

As one can see, a uniform distribution of model parameters allowed us to obtain a fairly good agreement between the simulation and observational results for both dependencies presented above. The situation is different for the relationship between characteristic wave spectral energy density of the QP element and the repetition period of emissions. Simulation results for the full set of model parameters are plotted in Figure 4a. Solid red line corresponds to the median of the frequency drift rate, and dashed red lines correspond to the lower and upper quartiles.

Comparing this result with the results of observation data analysis presented in Figure 7a in Hayosh et al. (2014), one can see the obvious

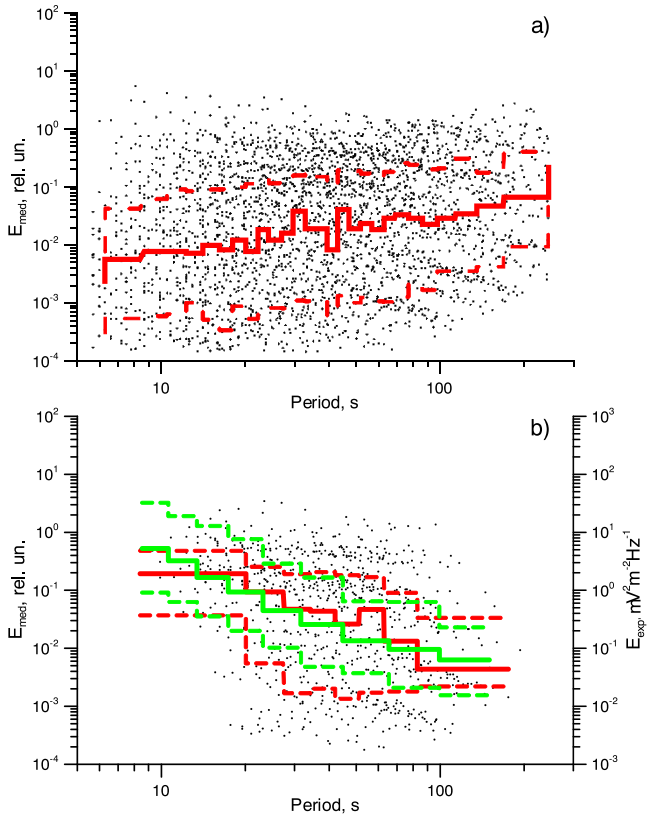


Figure 4. The dependence of the characteristic spectral energy density of waves in a quasiperiodic element on the period of emissions obtained from the results of numerical simulations, (a) for the entire set of simulation variants and (b) for the variants selected by constraint (8) on the cold plasma density. Solid red lines correspond to the median of the wave spectral energy density, and dashed red lines correspond to the lower and upper quartiles. Similar to Figure 2, solid and dashed green lines on (b) show, respectively, the median and the lower and upper quartiles for the corresponding statistical results of Hayosh et al. (2014).

inconsistency: Decrease in wave spectral energy density with increasing period of QP emissions was obtained from observation data, and the opposite trend is seen in Figure 4a.

An analysis of this inconsistency revealed that it can be removed by a proper choice of cold plasma density values for the simulations. Indeed, the density decreases with L in the magnetosphere, and it should be taken into account when choosing the simulation parameters.

In Figure 4b, the similar dependence as in Figure 4a is shown for a subset of all simulations selected by applying the following constraint:

$$N_{cL} = 200[\mathrm{cm}^{-3}] \cdot (4/L)^4 \pm 50\%. \tag{8}$$

In this case the relationship between the wave spectral energy density and QP period obtained in our simulations agrees with the results of observation data analysis plotted as green lines in Figure 4b: A general trend of the dependence is the same (a decrease in wave spectral energy density with increasing period), and the variation of the wave spectral energy density occurs in the same range of about 4 orders of magnitude.

Note that the exact form of condition (8) is not very important as long as it roughly corresponds to a realistic profile of equatorial cold plasma density, that is, a sufficiently fast decrease of cold plasma density with increasing L. The considered spread of N_{cL} in (8) actually includes the values obtained from popular plasmaspheric electron density models (see, e.g., Ozhogin et al., 2012).

Rather, wide spread of N_{cL} taken in (8) is also related to the fact that, according to the FCM model, generation of QP emissions usually occurs in regions with enhanced cold plasma density, such as magnetospheric ducts.

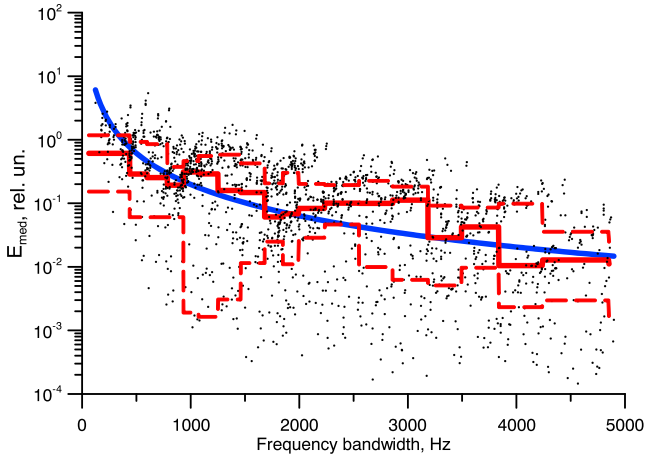


Figure 5. The dependence of the characteristic spectral energy density of waves in a quasiperiodic element on the frequency bandwidth obtained from the results of numerical simulations for the entire set of simulation variants. Solid red lines correspond to the median of the wave spectral energy density, and dashed red lines correspond to the lower and upper quartiles. Blue line is a power law approximation with the exponent equal to −1.65.

We assume that the duct parameters follow the same trend as the plasmaspheric density but can vary in a wide range.

Importantly, the use of constraint (8) for selecting simulation runs does not impede the simulation-observation agreement for the relationship between the frequency bandwidth and central frequency (Figure 2). Similar situation takes place for the relationship between the frequency drift rate of a QP element and the period of emissions. Use of constraint (8) leads to a decrease in the exponent value for a power law approximation which takes a value of about −1.07 in this case. This result coincides even better with the value of −1.2 obtained from the observation data by Hayosh et al. (2014).

The relationship between the characteristic wave spectral energy density and the frequency bandwidth of QP emissions is shown in Figure 5. The dependence is plotted for the entire set of simulation parameters. Solid red line corresponds to the median of wave spectral energy density, and dashed red lines correspond to its lower and upper quartiles. Blue line is a power law least-square approximation with the exponent equal to −1.65. A general trend of a decrease in wave spectral energy density with increasing frequency bandwidth is seen in the plot. A similar trend occurs in the case when constraint (8) is used for restricting simulation parameters (exponent value for a power law approximation takes a value of −1.8 in this case). The results obtained from numerical simulations do not agree with statistical analysis of observation data, where an inverse relationship was found.

4. Discussion

As one can see, the simulated interrelationships between the frequency bandwidth and central frequency and the frequency drift rate and the repetition period are in a fairly good agreement with the observational results even in the case of a uniform distribution of model parameters. This indicates a universal nature of the discussed scalings, which holds for all regimes realized in the simulations.

In particular, from the relation between the frequency bandwidth and central frequency (Figure 2), one can see that both values remain approximately equal to each other for the majority of parameter sets, which can be explained by the fact that the characteristic frequency scales of QP emission are determined by the frequency ω_0 (see equation (7)). Following from the relation between the frequency drift rate and the repetition period, it is seen that the frequency bandwidth (estimated as $\Delta f \approx T\mathrm{d}f/\mathrm{d}t$) weakly depends on the repetition period.

In contrast, an agreement for the relationship between the wave spectral energy density and the repetition period of QP emissions was obtained only by taking into account a realistic dependence of $N_{cL}(L)$. Let us consider the relations between the properties of QP emissions by using analytical estimates based on the quasi-linear equations. Using these equations (Trakhtengerts & Rycroft, 2008) and assuming that characteristic wave frequency is ω_0 (see equation (7)), it is possible to roughly estimate the characteristic value of the QP element spectral energy density as

$$\varepsilon_0 \approx \frac{J_0 W_0}{V_{\mathrm{gr}} |\ln R| \omega_{HL}}, \tag{9}$$

where J_0 is the energetic particle source intensity; V_{gr} is the wave group velocity. The parameter J_0 can be estimated as $J_0 \approx N_h/\tau_D$, where τ_D is a characteristic time of energetic electron drift across the generation region. Using the whistler wave group velocity approximation $V_{\mathrm{gr}} \approx 2c\sqrt{\omega_{HL}\omega}/\omega_{pL}$ and taking into account that $\tau_D \propto (LW_0)^{-1}$, we obtain the following relation between the characteristic wave spectral energy density and model parameters (hereafter all constants and numerical factors are omitted):

$$\varepsilon_0 \propto \frac{N_h v_0^5 L}{|\ln R|} \frac{\omega_{pL}^2}{\omega_{HL}^3} \propto \frac{N_h v_0^5}{|\ln R|} N_{cL} L^{10}. \tag{10}$$

In the regime of self-sustained oscillations with a duty cycle not significantly smaller than unity (i.e., when the pulse and pause durations are close to each other), the period of succession of QP elements can be estimated as a pulse duration which, in turn, is of the same order as an inverse value of the threshold growth rate: $t_p \approx T_{gr}/|\ln R|$ (see, e.g., Demekhov & Trakhtengerts, 1994, for details). Thus, using the same estimation for V_{gr} as above, we obtain the following dependence of repetition period on model parameters:

$$T \propto \frac{Lv_0}{|\ln R|\omega_{HL}} \propto \frac{v_0}{|\ln R|}L^4. \tag{11}$$

The characteristic frequency bandwidth can be estimated as $\Delta f \approx 2\pi\omega_0$ and the frequency drift rate as $\mathrm{d}f/\mathrm{d}t \approx \Delta f/T$, which gives the following relations for these values with the model parameters:

$$\Delta f \propto \frac{\omega_{HL}^3}{\omega_{pL}^2 v_0^2} \propto \frac{1}{v_0^2}N_{cL}L^{-9}, \tag{12}$$

$$\mathrm{d}f/\mathrm{d}t \propto \frac{|\ln R|\omega_{HL}^4}{L\omega_{pL}^2 v_0^3} \propto \frac{|\ln R|}{v_0^3}N_{cL}L^{-13}. \tag{13}$$

It is seen from equations (10)–(13) that all considered properties of QP emissions depend strongly on L-shell, whereas the dependence on other parameters is not so sharp. In the case where all model parameters (N_{cL}, W_0, N_h, and $|\ln R|$) are assumed independent on L, the following scalings are obtained:

$$\varepsilon_0 \propto L^{10}, \quad \Delta f \propto L^{-9}, \quad \mathrm{d}f/\mathrm{d}t \propto L^{-13}, \tag{14}$$

(assuming that the variation in the other model parameters leads to a quasi uniform spread of values).

In the case, where constraint (8) is used, we obtain

$$\varepsilon_0 \propto L^6, \quad \Delta f \propto L^{-5}, \quad \mathrm{d}f/\mathrm{d}t \propto L^{-9}. \tag{15}$$

For the repetition period in both cases, we have

$$T \propto L^4. \tag{16}$$

Equations (14) and (15) can be used to estimate the general trends in the relation of QP emission properties (bearing in mind that these estimates are fairly crude and the variations in the other parameters lead to a notable spread of values):

(i) The frequency drift rate $\mathrm{d}f/\mathrm{d}t$ should decrease with increasing the period T in both cases with a power law exponent of about -3 to -2 . Such a decreasing dependence qualitatively coincides with the results of numerical simulations (see Figure 3) and with the results of observation data analysis by Hayosh et al. (2014), though the exponent value is overestimated by a factor of about 2. Applying the constraint (8) leads to a decrease in the absolute value of the exponent, which agrees with the results of numerical simulations (see section 3.2). Recall that it also improves the agreement between the observations and simulation results; thus, the importance of taking into account density variation with L is confirmed by both simulations and analytical estimates. Opposite signs of exponents in the dependences of $\mathrm{d}f/\mathrm{d}t$ and T on L ensure that the variations in the other parameters do not change the qualitative trend in this relation.

(ii) Relations (14) and (15) yield, respectively, rough estimations $\varepsilon_0 \propto \Delta f^{-1.1}$ and $\varepsilon_0 \propto (df/dt)^{-1.2}$. Thus, in both cases, the characteristic wave spectral energy density ε_0 should decrease with increasing the frequency bandwidth Δf in both cases with a power law exponent of about -2 to -1. This is also in a good agreement with the simulation results obtained, where power law exponent was equal to -1.65 (see Figure 5). Similar to said above, variations in the other parameters should not change the general trend in this relation. These theoretical results, however, significantly disagree with observations by Hayosh et al. (2014) who observe an opposite trend.

(iii) Comparing (14) and (15) with (16), one can see that ε_0 should increase with increasing period T: $\varepsilon_0 \propto T^{2.5}$ and $\varepsilon_0 \propto T^{1.5}$ for (14) and (15), respectively. Therefore, the simple analytical estimates given above do not fully agree with the more accurate numerical results. However, the power law exponent of the analytical dependence $\varepsilon_0(T)$ decreases sharply (from 2.5 to 1.5) if we apply constraint (8). A similar decrease is seen in the case of numerical simulations, but in the latter case, the dependence becomes decreasing, that is, the effect of constraint (8) is stronger in the numerical model.

Concerning the contradiction between experimental and theoretical results for relationship between characteristic wave spectral energy density and the frequency bandwidth, to our mind, it can be related to the fact that data from low altitude observation of QP emissions were used in statistical study by Hayosh et al. (2014). As it was mentioned above, this means that emissions was observed far away from the generation region located near the equatorial plane. Due to the propagation effect, a frequency band and a wave amplitude at lower altitudes can differ strongly from those in the generation region. The FCM model operates only with values in the source region. Moreover, as is seen from the examples of QP emissions presented by Hayosh et al. (2014), the upper and lower frequencies of QP emissions can substantially vary during a single event from one QP element to another. Thus, a direct comparison of the results from observation and modeling for those properties of QP emission can be problematic.

Note that the other emission properties discussed above, such as their period and frequency drift rate, are almost unaffected by the wave propagation. The reason for that is that typical time scales of the QP emissions are much longer than the one-hop wave propagation time, so the group velocity dispersion cannot change the dynamical spectrum significantly.

5. Conclusions

We compared the interrelationships between the parameters of QP emissions obtained by Hayosh et al. (2014) with the results of numerical simulations based on the FCM model. Most of the observation results are in a good agreement with the simulations.

In particular, both observations and numerical simulations demonstrate an increase of frequency bandwidth with an increase of central frequency of QP emissions. A decrease of the frequency drift rate of QP elements with increase in period of QP emissions is also confirmed. Both these dependencies coincide for an arbitrary choice of model parameters.

A decrease of the characteristic wave spectral energy density with the increase in the emission period is also confirmed by modeling, but it requires correct choice of model parameters: a decrease of cold plasma density with increasing L-shell in the real condition should be taken into account. The obtained observational and numerical scaling is shown to be consistent with simplified analytical estimates based on the quasi-linear theory.

An agreement between the observations and simulations was not obtained for the relationship between the characteristic wave spectral energy density and the frequency band of QP emissions. We think this most probably can be explained by the influence of wave propagation from the generation region to the observation point, which strongly affects both the frequency band and wave spectral energy density. It will be important to perform a similar comparison with a statistical study based on the observations in the wave generation region, which is left for future work.

Acknowledgments
The work of D. P. and A. D. was supported by the Russian Science Foundation (project 15-12-20005). Simulation of specific events (section 3.1) was supported by the Ministry of Science and Higher Education of the Russian Federation (state task 0035-2014-0029). The work of F. N. was supported by Czech Science Foundation (GACR) grant 18-00844S. M. H. and O. S. were supported by the Praemium Academiae award from the Czech Academy of Sciences. DEMETER data are accessible online (https://sipad-cdpp.cnes.fr).

References

Bespalov, P. A. (1981). Self-modulation of radiation of a plasma cyclotron maser. *Journal of Experimental and Theoretical Physics Letters*, *33*(4), 182–185.

Bespalov, P. A., Parrot, M., & Manninen, J. (2010). Short-period VLF emissions as solitary envelope waves in a magnetospheric plasma maser. *Journal of Atmospheric and Solar-Terrestrial Physics*, *72*(17), 1275–1281. https://doi.org/10.1016/j.jastp.2010.09.001

Bespalov, P. A., & Trakhtengerts, V. Y. (1976). Dynamics of the cyclotron instability in a mirror system. *Soviet Journal of Plasma Physics*, *2*(3), 215–221.

Bösinger, T., Kaila, K., Rasinkangas, R., Pollari, P., Kangas, J., Trakhtengerts, V. Y., et al. (1996). An EISCAT study of a pulsating auroral arc: (i) Simultaneous ionospheric electron density, auroral luminosity and magnetic field pulsations. *Journal of Atmospheric and Terrestrial Physics*, *58*(1), 23–35.

Chen, L. (1974). Theory of ULF modulation of VLF emissions. *Geophysical Research Letters*, *1*(2), 73–75. https://doi.org/10.1029/GL001i002p00073

Davidson, G. T. (1979). Self-modulated VLF wave-electron interactions in the magnetosphere: A cause of auroral pulsations. *Journal of Geophysical Research*, *84*(A11), 6517–6523.

Demekhov, A. G., & Trakhtengerts, V. Y. (1994). A mechanism of formation of pulsating aurorae. *Journal of Geophysical Research*, *99*(4), 5831–5841.

Hanzelka, M., Santolík, O., Hajoš, M., Němec, F., & Parrot, M. (2017). Observation of ionospherically reflected quasiperiodic emissions by the DEMETER spacecraft. *Geophysical Research Letters*, *44*, 8721–8729. https://doi.org/10.1002/2017GL074883

Hayakawa, M., & Sazhin, S. S. (1992). Mid-latitude and plasmaspheric hiss: A review. *Planetary and Space Science*, *40*, 1325–1338.

Hayosh, M., Němec, F., Santolík, O., & Parrot, M. (2016). Propagation properties of quasiperiodic VLF emissions observed by the DEMETER spacecraft. *Geophysical Research Letters*, *43*, 1007–1014. https://doi.org/10.1002/2015GL067373

Hayosh, M., Němec, F., Santolík, O., & Parrot, M. (2014). Statistical investigation of VLF quasiperiodic emissions measured by the DEMETER spacecraft. *Journal of Geophysical Research: Space Physics*, *119*, 8063–8072. https://doi.org/10.1002/2013JA019731

Helliwell, R. A. (1965). *Whistlers and related ionospheric phenomena*. Palo Alto, Calif: Stanford Univ.Press.

Kimura, I. (1974). Interrelation between VLF and ULF emissions. *Space Science Reviews*, *16*(3), 389–411. https://doi.org/10.1007/BF00171565

Lyubchich, A. A., Demekhov, A. G., Titova, E. E., & Yahnin, A. G. (2017). Amplitude–frequency characteristics of ion–cyclotron and whistler-mode waves from Van Allen Probes data. *Geomagnetism and Aeronomy*, *57*(1), 40–50. https://doi.org/10.1134/S001679321701008X

Manninen, J., Demekhov, A. G., Titova, E. E., Kozlovsky, A. E., & Pasmanik, D. L. (2014). Quasiperiodic VLF emissions with short-period modulation and their relationship to whistlers: A case study. *Journal of Geophysical Research: Space Physics*, *119*, 3544–3557. https://doi.org/10.1002/2013JA019743

Manninen, J., Kleimenova, N., Turunen, T., & Gromova, L. (2018). New high-frequency (7–12 kHz) quasi-periodic VLF emissions observed on the ground at $L \sim 5.5$. *Annales Geophysicae*, *36*(3), 915–923. https://doi.org/10.5194/angeo-36-915-2018

Manninen, J., Turunen, T., Kultima, J., & Titova, E. (1994). Correlating optical emissions, quasi-periodic very low frequency emission and magnetic Pc3 pulsations. *Geomagnetism and Aeronomy*, *34*, 42–47.

Morrison, K. (1990). Quasi-periodic VLF emissions and concurrent magnetic pulsations seen at L = 4. *Planetary and Space Science*, *38*(12), 1555–1565. https://doi.org/10.1016/0032-0633(90)90161-I

Němec, F., Bezděková, B., Manninen, J., Parrot, M., Santolík, O., Hayosh, M., & Turunen, T. (2016). Conjugate observations of a remarkable quasiperiodic event by the low-altitude DEMETER spacecraft and ground-based instruments. *Journal of Geophysical Research: Space Physics*, *121*, 8790–8803. https://doi.org/10.1002/2016JA022968

Němec, F., Hospodarsky, G. B., Bezděkovà, B., Demekhov, A. G., Pasmanik, D. L., Santolík, O., et al. (2018). Quasiperiodic whistler mode emissions observed by the Van Allen Probes spacecraft. *Journal of Geophysical Research: Space Physics*, *123*, 8969–8982. https://doi.org/10.1029/2018JA026058

Němec, F., Hospodarsky, G., Pickett, J. S., Santolík, O., Kurth, W. S., & Kletzing, C. (2016). Conjugate observations of quasiperiodic emissions by the Cluster, Van Allen Probes, and THEMIS spacecraft. *Journal of Geophysical Research: Space Physics*, *121*, 7647–7663. https://doi.org/10.1002/2016JA022774

Němec, F., Pickett, J. S., & Santolík, O. (2014). Multispacecraft Cluster observations of quasiperiodic emissions close to the geomagnetic equator. *Journal of Geophysical Research: Space Physics*, *119*, 9101–9112. https://doi.org/10.1002/2014JA020321

Němec, F., Santolík, O., Pickett, J. S., Parrot, M., & Cornilleau-Wehrlin, N. (2013). Quasiperiodic emissions observed by the Cluster spacecraft and their association with ULF magnetic pulsations. *Journal of Geophysical Research: Space Physics*, *118*, 4210–4220. https://doi.org/10.1002/jgra.50406

Ozhogin, P., Tu, J., Song, P., & Reinisch, B. W. (2012). Field-aligned distribution of the plasmaspheric electron density: An empirical model derived from the IMAGE RPI measurements. *Journal of Geophysical Research*, *117*, A06225. https://doi.org/10.1029/2011JA017330

Pasmanik, D. L., Demekhov, A. G., Trakhtengerts, V. Y., & Parrot, M. (2004a). Modeling whistler wave generation regimes in magnetospheric cyclotron maser. *Annales Geophysicae*, *22*, 3561–3570. https://doi.org/10.5194/angeo-22-3561-2004

Pasmanik, D. L., Demekhov, A. G., Trakhtengerts, V. Y., & Parrot, M. (2004b). Quasi-periodic ELF/VLF wave emissions in the Earth's magnetosphere: Comparison of satellite observations and modeling. *Annales Geophysicae*, *22*, 4351–4361. https://doi.org/10.5194/angeo-22-4351-2004

Sato, N., & Fukunishi, H. (1981). Interaction between ELF–VLF emissions and magnetic pulsations: Classificaton of quasi-periodic ELF–VLF emissions based on frequency-time spectra. *Journal of Geophysical Research*, *86*(A1), 19–29.

Sato, N., Hayashi, K., Kokubun, S., Oguti, T., & Fukunishi, H. (1974). Relationship between quasi-periodic VLF-emission and geomagnetic pulsation. *Journal of Atmospheric and Terrestrial Physics*, *36*(9), 1515–1526.

Sazhin, S. (1987). An analytical model of quasiperiodic ELF-VLF emissions. *Planetary and Space Science*, *35*(10), 1267–1274. https://doi.org/10.1016/0032-0633(87)90111-5

Sazhin, S. S., & Hayakawa, M. (1994). Periodic and quasiperiodic VLF emissions. *Journal of Atmospheric and Terrestrial Physics*, *56*(6), 735–753.

Smith, A. J., Engebretson, M. J., Klatt, E. M., Inan, U. S., Arnoldy, R. L., & Fukunishi, H. (1998). Periodic and quasiperiodic ELF/VLF emissions observed by an array of Antarctic stations. *Journal of Geophysical Research*, *103*, 23,611–23,622.

Titova, E. E., Kozelov, B. V., Demekhov, A. G., Manninen, J., Santolík, O., Kletzing, C. A., & Reeves, G. (2015). Identification of the source of quasiperiodic VLF emissions using ground-based and Van Allen Probes satellite observations. *Geophysical Research Letters*, *42*, 6137–6145. https://doi.org/10.1002/2015GL064911

Trakhtengerts, V. Y., & Rycroft, M. J. (2008). *Whistler and Alfven mode cyclotron masers in space, Cambridge Atmospheric and Space Science Series*. Cambridge, UK: Cambridge University Press. https://doi.org/10.1017/CBO9780511536519

Trakhtengerts, V. Y., Tagirov, V. R., & Chernous, S. A. (1986). A circulating cyclotron maser and impulsive VLF emissions. *Geomagnetism and Aeronomy*, *26*(1), 77–82.